Mon. Not. R. Astron. Soc. **393,** L1–L5 (2009) doi:10.1111/j.1745-3933.2008.00580.x

The *XMM–Newton* long look of NGC 1365: uncovering of the obscured X-ray source

G. Risaliti,[1,2⋆] M. Salvati,[2] M. Elvis,[1] G. Fabbiano,[1] A. Baldi,[1] S. Bianchi,[3] V. Braito,[8,9] M. Guainazzi,[5] G. Matt,[3] G. Miniutti,[6] J. Reeves,[4] R. Soria[7] and A. Zezas[1]

[1]*Harvard–Smithsonian Center for Astrophysics, 60 Garden Street, Cambridge, MA 02138, USA*
[2]*INAF – Osservatorio di Arcetri, L.go E. Fermi 5, Firenze, Italy*
[3]*Dipartimento di Fisica, Università degli Studi 'Roma Tre', Via della Vasca Navale 84, I-00146 Roma, Italy*
[4]*Astrophysics Group, School of Physical and Geographical Science, Keele University, Keele, Staffordshire ST5 5BG*
[5]*European Space Astronomy Centre of ESA, Apartado 50727, E-28080 Madrid, Spain*
[6]*Laboratoire Astroparticule et Cosmologie (APC), UMR 7164, 10 Rue A. Domon et L. Duquet, 75205 Paris, France*
[7]*MSSL, University College London, Holmbury St. Mary, Dorking, Surrey, RH5 6NT*
[8]*Department of Physics and Astronomy, University of Leicester, University Road, Leicester, LE1 7RH*
[9]*Department of Physics and Astronomy, John Hopkins University, Baltimore, MD 21218, USA*

Accepted 2008 October 23. Received 2008 October 23; in original form 2008 July 28

ABSTRACT

We present an analysis of the extreme obscuration variability observed during an *XMM–Newton* 5-d continuous monitoring of the active galactic nuclei (AGN) in NGC 1365. The source was in a reflection-dominated state in the first ∼1.5 d, then a strong increase in the 7–10 keV emission was observed in ∼10 h, followed by a symmetric decrease. The spectral analysis of the different states clearly shows that this variation is due to an uncovering of the X-ray source. From this observation, we estimate a size of the X-ray source $D_S < 10^{13}$ cm, a distance of the obscuring clouds $R \sim 10^{16}$ cm and a density $n \sim 10^{11}$ cm^{-3}. These values suggest that the X-ray absorption/reflection originates from the broad-line region clouds. This is also supported by the resolved width of the iron narrow $K\alpha$ emission line, consistent with the width of the broad Hβ line.

Key words: galaxies: individual: NGC 1365.

1 INTRODUCTION

The structure, size and physical properties of the circumnuclear medium of active galactic nuclei (AGN) are still a matter of debate and investigation. The axisymmetric (torus-like) geometry required by AGN unified models (e.g. Antonucci 1993) can be obtained by means of quite different structures, from galactic dust lanes to subparsec scale, high-density tori. In this context, the hard X-ray observations of the nearby obscured Seyfert Galaxy NGC 1365 have proven to be a unique opportunity to investigate the properties of the AGN circumnuclear medium, as well as to put tight constraints on the size of the X-ray source.

NGC 1365 is a nearby ($z = 0.0055$) Seyfert 1.8 Galaxy. Several observations performed in the hard X-rays in the past ∼15 yr with all the major X-ray observatories revealed several spectral changes from Compton-thin to reflection-dominated states, implying an extraordinary absorption variability from $N_H \sim 10^{23}$ cm^{-2} to $N_H > 10^{24}$ cm^{-2} (Risaliti et al. 2005a; Risaliti et al. 2007, hereafter R05A and R07, respectively). The most extreme variations have been observed during a recent *Chandra* campaign consisting of six short (15 ks) observations performed in 10 d. The source was in a Compton-thin state during the first observations, then 'disappeared' (i.e. only the reflected component was visible) in the second observation two days later, and was back in the initial state during the third and later observations. The interpretation of this extreme variability is based on the presence of Compton-thick eclipsing clouds crossing the line of sight to the central source. We discussed this scenario in R07 where we obtained stringent constraints on the X-ray source size ($D < 10^{14}$ cm) and, under the hypothesis of Keplerian motion of the eclipsing clouds, on the distance of the absorber from the central black hole ($R \leq 10^{16}$ cm).

The main limits of this analysis are the lack of continuous monitoring during the eclipse, and the relatively low signal-to-noise ratio (S/N) of the *Chandra* spectra, due to the low-effective area at high energies ($E > 2$ keV) and the short observing time. In order to solve these problems, we obtained a 5-d *XMM–Newton* almost continuous look of NGC 1365. During this observation, the source was on average in a low flux, reflection-dominated state. However, a dramatic spectral change was observed after ∼2 d, when a hard

⋆E-mail: grisaliti@cfa.harvard.edu

transient component appeared for ∼60 ks. In this Letter, we present the analysis of this *XMM–Newton* long look of NGC 1365, and we focus on the implications of the observed absorption variability.

2 DATA REDUCTION AND ANALYSIS

The observation was performed from 2007 May 30 to June 5. for three complete orbits (1384–1386). The reduction and calibration were performed with the SAS package, following standard procedures as recommended by the *XMM–Newton* Science Operation Center.

We included all the time intervals in the timing and spectral analysis, except for the final ∼15 ks of the second orbit, when high background flares saturated the EPIC detectors. The spectra and light curves were extracted from a circular region with a 25 arcsec radius. With this choice, the background level is always lower than 5 per cent of the source spectrum at all times and energy intervals. For both the timing and spectral analysis, we always used the complete PN and MOS (merged) set of data, which are fully consistent with each other. In the figures, however, we only show the PN data, for clarity.

In Fig. 1, we show the low- (2–5 keV) and high-energy (7–10 keV) light curves obtained from the PN. A visual analysis of these curves reveals a strong variation during the first-half of the second orbit, consisting of an increase in the hard flux, followed by a symmetric decrease. The hard flux in the second-half of the second and third orbit remains constant, at a level slightly higher than in the first orbit. At low energies, the source remains constant throughout the observation. Considering the past observed fast absorption changes, the most likely interpretation of this variability is a transient decrease in the absorbing column density during the second orbit.

In order to test this hypothesis and to perform a complete spectral analysis of our data, we extracted the spectra from six time intervals, corresponding to different spectral states, as shown in Fig. 1 (the fifth and sixth intervals show no obvious variations, and are separated only because they belong to two different orbits). The spectral analysis was performed with the XSPEC 12.4 package (Arnaud 1996).

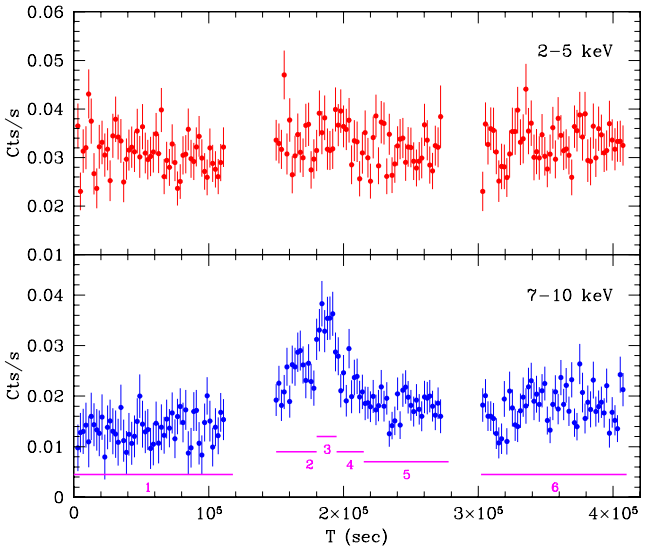

Figure 1. 2–5 keV (top panel) and 7–10 keV (bottom panel) light curves of the nuclear emission of NGC 1365 during the *XMM–Newton* long look. The horizontal segments show the extraction time intervals for the six spectra discussed in the text.

Here, we are only interested in the variations observed in the high-energy ($E > 2$ keV) emission. Therefore, we do not discuss in detail the lower energy (0.5–2 keV) emission, which has a diffuse origin, as shown by *Chandra* images (R05A). However, this component cannot be completely neglected for two reasons: (i) an analysis of the *Chandra* diffuse emission shows a faint, but not negligible, tail at energies higher than 2 keV and (ii) the fits of the high-energy spectra should not include components whose extrapolations towards low energies overpredict the observed emission. In order to take into account these aspects, we extracted a spectrum of the diffuse emission from the total *Chandra* data, in an annulus centered on the nucleus, with external radius equal to that used in the *XMM–Newton* analysis, and inner radius of two arcsec, in order to remove the central emission. We then fitted this spectrum with a multicomponent model providing a good analytical representation of the data. The analysis of the *XMM–Newton* spectra was performed adding to all models the fixed components found in the *Chandra* analysis, with a 5 per cent maximum range in the cross-calibration.

We first performed the analysis of the six intervals separately. The spectrum of the first interval can be entirely reproduced by a continuum reflection (PEXRAV model in XSPEC, Magdziarz & Zdziarski 1995) plus a set of three emission lines, at energies between 6.4 and 7.0 keV. The other five spectra are successfully reproduced with the same model as above, plus an intrinsic continuum component, consisting of an absorbed power law. The photon index, column density and flux of the intrinsic component were left free to vary for each spectrum. The slope of the incident continuum for the reflection component is assumed to be the same as that of the intrinsic emission. In all the cases, the parameters of the reflection continuum are compatible with the values found in the first spectrum. The column density and photon index of the intrinsic component are also constant within the errors, with values in the ranges $\Gamma \sim 2.3$–2.9 and $N_{\rm H} \sim 5$–10×10^{23} cm^{-2}. Instead, the flux shows strong variations.

As a second step in order to obtain a physically consistent view of the observed variability, we performed a simultaneous analysis of the six spectra, imposing constant reflection parameters. The photon index and the absorption column density of the intrinsic power law were also required to be constant, while the flux was left free to vary in all the six intervals. The best-fitting parameters are shown in Table 1. In Fig. 2, we show the three spectra from the first, third and sixth interval, and the residuals for all the intervals. It is clear from the overall goodness of fit and from the residual distribution, showing no obvious unaccounted features, that the adopted model provides a good representation of the spectral variations observed in Fig. 1.

Table 1. *XMM–Newton* analysis.

Γ	$2.76^{+0.37}_{-0.37}$	Norm 1[a]	$0.2^{+0.07}_{-0.07}$
N (Refl.)[a]	$0.73^{+0.4}_{-0.3}$	Norm 2[a]	$1.9^{+0.2}_{-0.2}$
$N_{\rm H}$[b]	94^{+10}_{-10}	Norm 3[a]	$2.8^{+0.3}_{-0.3}$
		Norm 4[a]	$1.8^{+0.2}_{-0.2}$
		Norm 5[a]	$0.8^{+0.1}_{-0.1}$
χ^2/d.o.f.	1799/1711	Norm 6[a]	$0.8^{+0.1}_{-0.1}$

[a]Normalizations of the reflected component (constant in all intervals) and the transmitted components in each of the six intervals shown in Fig. 1, in units of 10^{-3} keV s^{-1} cm^{-2} keV^{-1}.
[b]Absorbing column density of the intrinsic component, in units of 10^{22} cm^{-2}.

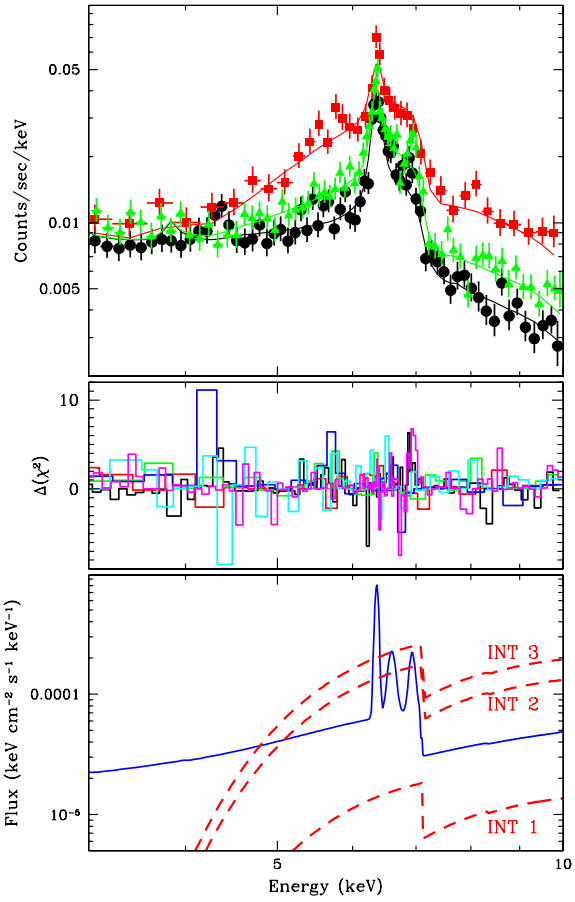

Figure 2. Upper panel: PN Spectra obtained from the time intervals 1, 3 and 6 as shown in Fig. 1. The increase in the interval 3 spectrum (red diamonds) and, in a smaller fraction, in the interval 6 spectrum (green triangles) are well reproduced by an intrinsic power-law continuum absorbed by a column density $N_{\rm H} \sim 9 \times 10^{23}$ cm^{-2} (see the text for details). The other three PN and six MOS spectra are not shown for clarity, but are fully discussed in the text. Middle panel: contribution to χ^2 for each of the six spectra, showing no significant feature not included in the model. Lower panel: best-fitting model components for the first, second and third interval. The continuous lines are common to all intervals, and represent the reflected components. The dashed lines show the intrinsic component, negligible in the first interval, showing up in the second interval and further increasing in the third.

3 DISCUSSION

The spectral analysis presented above shows that the observed high-energy variations are due to a power-law component, absorbed by a column density $N_{\rm H} \sim 9 \times 10^{23}$ cm^{-2}, rising from approximately 0 up to its maximum flux in ∼30 ks, and then decreasing down to ∼20 per cent of its maximum in a similar time. These observations can be interpreted as due to intrinsic continuum variability, or to a change in the absorbing column density along the line of sight. The former case would imply a switch-on of the X-ray source from an almost completely reflection-dominated state (Table 1) in ∼30 ks, followed by a strong decrease in a similar time. Such short time-scales are unlikely in a disc-corona scenario, as discussed in R05A, however they cannot be completely ruled out. On the other side, absorption variability is a most likely scenario in this case, given the X-ray observational history of NGC 1365:

(i) Unequivocal column density variations in short times-scales (<2 d) have been observed during the *Chandra* campaign (R07). Here, we refer, in particular, to the Compton-thin variations occurred during the last four observations, which cannot be interpreted as due to intrinsic continuum variability.

(ii) Another transit of an obscuring cloud has been detected in a previous *XMM–Newton* 60 ks observation (Risaliti et al. 2008). In this case, the crossing cloud does not completely cover the source, and its column density is $\sim 3 \times 10^{23}$ cm^{-2}. This makes the spectral analysis more complicated than in our case. However, the eclipsing time is of the same order as that observed here, while the underlying continuum remains constant.

(iii) Considering all the past X-ray observations where the source was in a Compton-thin state, strong variations of the primary continuum have never been observed: the estimated intrinsic flux is constant within a factor of at most 2.

Based on these arguments, we conclude that the interpretation invoking absorption variability is the most appropriate for our observations. Within this scenario, thick clouds move along the line of sight, uncovering and then covering again the primary X-ray source. The covering factor of the thick clouds is almost complete during the first *XMM–Newton* orbit [Interval (INT) 1 in Fig. 1], then decreases to a minimum, and then increases again, leaving only ∼10 per cent of the source uncovered in INT 5 and 6. It is not possible from these observations to tell directly whether the uncovering is complete at the flux maximum. We note, however, that the extrapolated 2–10 keV flux in INT 3 [F(2–10) $\sim 3 \times 10^{-11}$ erg s^{-1} cm^{-2}, adopting the continuum parameters shown in Table 1] is compatible with the highest value measured in past observations (Risaliti et al. 2005b, hereafter R05B). This is an indication that most of the X-ray source is probably uncovered during INT 3.

Two schemes for the geometrical structure of the circumnuclear absorber are possible (Fig. 3).

(i) The Compton-thick absorber is made of clouds with about the same size of the source. On average, few (1–3) of these clouds cross the line of sight. Depending on the fluctuations in the number and column density of the clouds, the source can be seen in a reflection-dominated state for most of the time, with a short interval in a Compton-thin state, as observed.

(ii) The thick clouds are bigger than the X-ray source by a factor of the order of the ratio between the continuous Compton-thick and Compton-thin intervals in our observation. In this case, our light curve can be reproduced by the crossing of a single thick cloud, followed by a short interval where only thin gas is present along the line of sight, followed by another 'big' thick cloud.

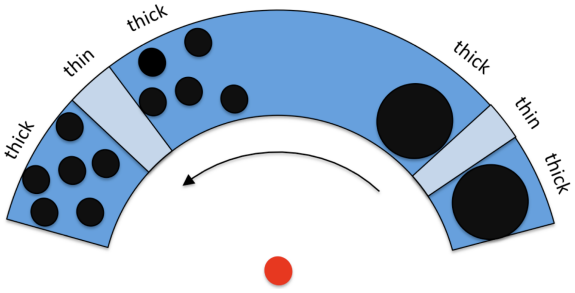

Figure 3. Possible models for the structure of the circumnuclear absorber. The black points represent Compton-thick clouds. The regions with a darker background in the 'torus' are those where at least one thick cloud crosses the line of sight to the X-ray source (the red spot in the centre). The regions with a lighter background show the Compton-thin lines of sight.

The observations discussed here can only constrain the properties of the thick clouds, but nothing can be directly inferred on the thin material. In principle, it can be in a different physical state (either homogeneous, or distributed in clouds of different size) and distance (either closer or farther) from the central source. The variations of Compton-thin absorption observed with *Chandra* (R07) in timescales of two days rule out a homogeneous material. Considerations on the ionization state (see below for more details) also rule out that the thin material is closer to the centre than the thick clouds. However, a layer of thin clouds external to the thick ones, or a co-spatial mix of thick and thin clouds, is possible.

In order to estimate the relevant geometrical and physical quantities (i.e. the size of the X-ray source, the size and distance from the centre of the obscuring clouds, their density), we first note that the covering/uncovering time depends only on the source size and velocity of the thick clouds, but not on the dimensions of the obscuring clouds, nor on the structure of the thin gas. If the covering clouds (for the remainder of the analysis, we always refer to the Compton-thick component only) have different velocities, the maximum size of the X-ray emitting region is still given by the velocity of the fastest cloud, v, times the eclipsing time, T. In R07, we discussed possible ways to constrain these two quantities.

(i) The time intervals between consecutive observations which caught the source in different states provided upper limits to the eclipsing time $T < 1$ d.

(ii) Two main arguments provided constraints to the cloud velocity: (i) a limit to the ionization state of the absorbing gas, which cannot be too highly ionized in order to effectively absorb the primary component and (ii) a limit on the width of the narrow iron emission line, under the assumption that reflection and absorption are due to the same physical component.

The new observations presented here allow an improved estimate of all the above constraints. (i) the eclipsing time T is directly measured from the observations ($T \sim 10$ h); (ii) the iron narrow emission line is now resolved and therefore the linewidth can be directly measured and (iii) having a precise determination of the reflection-dominated spectrum and a measurement of the intrinsic continuum from past observations (R05B) we can put a more stringent upper limit on the ionization parameter U of the obscuring cloud. Here, we discuss the linewidth and ionization parameter arguments, following the scheme of R07.

Ionization parameter. In order to obtain complete obscuration of the primary source, as observed in INT 1 (Fig. 1), the obscuring gas cannot be too highly ionized. The intrinsic continuum can be estimated from previous X-ray observations. In particular, the *XMM–Newton* observation of 2004 January, described in R05B, provided the lowest $N_{\rm H}$, highest S/N spectrum available. We therefore adopted the best-fitting continuum model from this observation as the intrinsic ionizing emission from the central X-ray source. We added this component to the best-fitting model for INT 1 and we allowed for ionized absorption, following the model by Done et al. (1992). In order to reproduce the observed spectrum without overpredicting the continuum, the ionization parameter must be $U < 20$ erg cm s^{-1} and the absorbing column density $N_{\rm H} > 2 \times 10^{24}$ cm^{-2}. From this limit, we can obtain upper limits on the source size and cloud distance from the center, R, under the assumption of Keplerian cloud velocity $v = (GM_{\rm BH}/R)^{1/2}$, and assuming that the cloud size $D_{\rm C}$ is larger than the size of the X-ray source $D_{\rm S}$. With simple algebra (see R07 for details) we obtain

$$R > (GM_{\rm BH})^{1/5}[TL_{\rm X}/(U_{\rm max}N_{\rm H})]^{2/5}, \quad (1)$$

Table 2. Line parameters.

Line	E (keV)	σ (eV)	EW[a] (eV)
1	$6.40^{+0.06}_{-0.05}$	30^{+14}_{-19}	800^{+70}_{-60}
2	$6.64^{+0.02}_{-0.04}$	58^{+34}_{-36}	180^{+45}_{-30}
3	$6.95^{+0.02}_{-0.02}$	<91	330^{+50}_{-60}

[a]EWs are estimated with respect to the reflection component.

where $L_{\rm X}$ is the ionizing 1–150 keV radiation, which we take from R05B: $L_{\rm X} = 1.5 \times 10^{42}$ erg s^{-1}. The central black hole mass, $M_{\rm BH}$, can been estimated through the relations between the black hole mass and (i) the bulge velocity dispersion [$\log(M_{\rm BH}/{\rm M}_\odot) = 7.3 \pm 0.4(0.3)$ Oliva et al. 1995; Ferrarese & Ford 2005] and (ii) the bulge luminosity in the K band [$\log(M_{\rm BH}/{\rm M}_\odot) = 7.8 \pm 0.4(0.3)$, Dong & De Robertis 2006; Marconi & Hunt 2003], where the two quoted errors refer to the statistical (systematic) effects. From these values, we obtain $R > 1.2 \times 10^{15}$ cm. The limits on the cloud velocity and the X-ray source size are $v = (GM_{\rm BH}/R)^{1/2} < 9,000\, M_7^{2/5}$ km s^{-1} and $D_{\rm S} < 2.7 \times 10^{13} M_7^{2/5}$ cm. This size can be expressed in units of gravitational radii, $R_{\rm G} = 2GM_{\rm BH}/c^2$, obtaining $D_{\rm S} < 10\, M_7^{-3/5}\, R_{\rm G}$.

Linewidth. The narrow emission lines present in all spectra are due to reflection by circumnuclear gas. It is reasonable to assume that the reflector and the absorbing clouds are the same physical component. This is supported by the occurrence of Compton-thick states in the past X-ray observations of NGC 1365, with a duty cycle of about one-third (Iyomoto et al. 1997; Risaliti, Maiolino & Bassani 2000, R05A, R07). It follows that the Compton-thick absorber covers approximately one-third of the solid angle, and therefore a significant reflection component must be produced by this gas. Interestingly, the ratio R between the normalizations of the reflection and intrinsic continuum components (Table 1) in the uncovered spectrum (INT 3) is about one-third, further supporting the identification between the reflector and the thick absorber. In this scenario, we can estimate the velocity of the obscuring cloud from the width of the narrow component of the neutral iron emission line. Thanks to its large equivalent width in reflection-dominated states, the long *XMM–Newton* observation allows a precise analysis of the line profile, and an estimate of its width. The line is resolved at the 4σ level [full width at half-maximum (FWHM)(Fe) = 3100^{+1500}_{-1900} km s^{-1}, Table 2]. The cloud velocity in the plane of the sky is then obtained by de-projecting the measured linewidth in spherical symmetry. The final estimate of the cloud velocity $v = 2100^{+1000}_{-1300}$ km s^{-1}. The linear dimension of the X-ray source is then $D_{\rm S} = 6^{+3}_{-4} \times 10^{12}$ cm. Using the black hole mass values discussed in the previous paragraph, and assuming Keplerian motion of the obscuring cloud, we find $R \sim 2.0 \pm 0.7 \times 10^{16}\, M_7^{1/5}$ cm and $D_{\rm S} = 2 \pm 1\, M_7^{-1}\, R_{\rm G}$.

In order to have a physically reasonable size of the X-ray source, $D_{\rm S} \sim 10 R_{\rm G}$, the black hole mass must be of the order of 2–3 $\times 10^6$ M$_\odot$. These values are consistent at a $\sim 1\ \sigma$ level with the mass estimate from the velocity dispersion–black hole mass correlation (see above in this section). The estimate from the bulge luminosity–black hole mass relation is instead higher at a 2 σ level, but this is expected due to the strong starburst contribution to the bulge luminosity of NGC 1365. A further indication of a black hole mass of the order of a few 10^6 M$_\odot$ comes from the $M_{\rm BH}$–Hβ width correlation (Kaspi et al. 2005). We obtained the width of the Hβ broad component

from Schulz et al. 1999, while the optical luminosity of the AGN component has been estimated from the X-ray 2 keV intrinsic luminosity (R05B), assuming a standard AGN SED (Spectral Energy Distribution) in the optical/ultraviolet (Risaliti & Elvis 2004) and the optical/X-ray ratio of Steffen et al. (2006). With these values $M_{\rm BH} = 2 \times 10^6\,{\rm M}_\odot$. This estimate is rather uncertain, both on the assumptions on the SED and on the use of the Kaspi et al. correlation down to a luminosity lower than those for which the correlation has been tested.

The above analysis, mainly focused on the size of the X-ray source, also suggests an identification between the thick circumnuclear reflector/absorber and the broad-line region. First, we note that the resolved velocity of the iron emission line is consistent with the width of the broad Hβ emission line [FWHM(H β) $\sim 1900\,{\rm km\,s^{-1}}$, Schulz et al. 1999], analogously to what recently found in another Seyfert Galaxy, NGC 7213, by means of *Chandra* grating spectroscopy (Bianchi et al. 2008). Further support to this identification comes from the estimate of the size $D_{\rm C}$ and density n of the obscuring clouds. As shown by the configurations in Fig. 3, $D_{\rm C}$ cannot be uniquely measured from our analysis. However, a cloud size much higher than the source size is unlikely from a geometrical point of view. This is also suggested by the relatively short duration (<2 d) of the eclipse observed with *Chandra* (R07). Assuming $D_{\rm C} = 1$–$3 \times D_{\rm S}$, and a column density $N_{\rm H} \sim 2 \times 10^{24}\,{\rm cm^{-2}}$, we obtain $n \sim 1$–$3 \times 10^{11}\,{\rm cm^{-3}}$, in agreement with the estimates for the broad-line clouds.

4 CONCLUSIONS

Our analysis clearly demonstrates two main points.

(i) The size of the X-ray source is $D_{\rm S} < 10^{13}$ cm, corresponding to a few gravitational radii.

(ii) The obscuring clouds have a distance from the centre and a density typical of the broad-line region. The measured iron emission linewidth is consistent with the width of the broad Hβ line. This further supports an identification between the X-ray reflector/absorber and the broad-line clouds.

Our estimates rely on a simplified scheme, with homogeneous spherical clouds moving with Keplerian velocity around the central source. Possible effects not considered in our analysis are a non-Keplerian component of the cloud velocity (e.g. due to an outflow), non-spherical geometries and possible $N_{\rm H}$ variations within the obscuring cloud. All these considerations make the actual numbers uncertain within a small factor, but do not change the two general conclusions listed above.

ACKNOWLEDGMENTS

We are grateful to the anonymous referee for his/her helpful comments. This work has been funded by NASA Grant NNX07AR90G.

REFERENCES

Antonucci R., 1993, ARA&A, 31, 473
Arnaud K. A., 1996, in Jacoby H. G., Barnes J., eds., ASP Conf. Ser. Vol. 101. Astron. Soc. Pac., San Francisco, p. 17
Bianchi S., La Franca F., Matt G., Guainazzi M., Jimenez Bailón E., Longinotti A. L., Nicastro F., Pentericci L., 2008, MNRAS, 389, L52
Done C., Mulchaey J. S., Mushotzky R. F., Arnaud K. A., 1992, ApJ, 395, 275
Dong X. Y., De Robertis M. M., 2006, AJ, 131, 1236
Ferrarese L., Ford H., 2005, Space Sci. Rev., 116, 523
Iyomoto N., Makishima K., Fukazawa Y., Tashiro M., Ishisaki Y., 1997, PASJ, 49, 425
Kaspi S., Maoz D., Netzer H., Peterson B. M., Vestergaard M., Jannuzi B. T., 2005, ApJ, 629, 61
Magdziarz P., Zdziarski A. A., 1995, MNRAS, 273, 837
Marconi A., Hunt L. K., 2003, ApJ, 589, L21
Oliva E., Origlia L., Kotilainen J. K., Moorwood A. F. M., 1995, A&A, 301, 55
Risaliti G., Elvis M., 2004, ASSL Vol. 308, Supermassive Black Holes in the Distant Universe. Kluwer, Dordrecht, p. 187
Risaliti G., Maiolino R., Bassani L., 2000, A&A, 356, 33
Risaliti G., Elvis M., Fabbiano G., Baldi A., Zezas A., 2005a, ApJ, 623, L93 (R05A)
Risaliti G., Bianchi S., Matt G., Baldi A., Elvis M., Fabbiano G., Zezas A., 2005b, ApJ, 630, L129 (R05B)
Risaliti G., Elvis M., Fabbiano G., Baldi A., Zezas A., Salvati M., 2007, ApJ, 659, L111 (R07)
Risaliti G. et al., 2008, ApJ, submitted
Schulz H., Komossa S., Schmitz C., Mücke A., 1999, A&A, 346, 764
Steffen A. T., Strateva I., Brandt W. N., Alexander D. M., Koekemoer A. M., Lehmer B. D., Schneider D. P., Vignali C., 2006, AJ, 131, 2826

This paper has been typeset from a TEX/LATEX file prepared by the author.